2005 유체기계 연구개발 발표회 논문집, pp. 533~541
창원대학교 국제교류센터 및 정보전산원, 2005. 12. 1~2

비대칭 팁간극이 원심압축기의 유동에 미치는 영향

윤용상* • 송성진**

Effects of Asymmetric Tip Clearance on Centrifugal Compressor Flow

Yong Sang Yoon* • Seung Jin Song**

Key Words : Centrifugal compresso (원심 압축기)r, Asymmetric tip clearance (비대칭 팁간극), Flow nonuniformity. (유동 불균일)

ABSTRACT

Compared to axial compressors, an analytical model capable of analyzing the flow in centrifugal compressor lacks because of the difficulty in governing equations for radial duct. Therefore, this paper presents a new model to predict flow field in a centrifugal compressor with a sinusoidal asymmetric tip clearance. To predict the 2 dimensional flow in the inlet and exit of the centrifugal compressor, the two flow fields are connected with compressor characteristic based on Moore-Greitzer model. Contrary to axial compressors, the nonuniformity of impeller exit pressure in centrifugal compressor decreases as flow coefficient decreases. In addition, that is sensitive to the slope of pressure rise by eccentricity. The maximum velocity exists right before the maximum tip clearance.

1. Introduction

Tip clearance flow plays an important role in a compressor performance and stability. Tip leakage flow rolls up into a tip vortex to make a blockage in a passage and to generate a loss. As the tip clearance is increased, the pressure rise, efficiency, and stall margin are degraded. Circumferential asymmetric flow due to inlet distortion, casing eccentricity, and rotor shaft eccentricity also induces problems in turbomachinery. For example, it causes rotor shaft bending, whirling, and so on. Initially, the destabilizing effects of rotor tip clearance asymmetry on turbine rotors were suggested by Thomas [1] and Alford [2]. They suggested that an asymmetric tip clearance destabilizes forward whirl-inducing force.

Modeling for compression system usually is used for understanding a surge and a rotating stall dynamics. Initially, Greitzer [3] has revealed the B-parameter which describes surge dynamics. Moore and Greitzer [4] suggested new 2 dimensional model in time variation to explain rotating stall. Based on Greizer's and Moore-Greitzer's model, many researches in instability and stability control have been done. Hynes and Greitzer [5] presented a compressor stability model to assess the effect of inlet flow distortion. Graf et al. [6] extended their model and experimentally showed the nonuniformity in axial velocity to verify their own model. Gordon [7] developed Graf's model to account for the

Table 1 Dimensions for axial and centrifugal compressor

	Axial	Centrifugal
Rt1 (Tip radius, m)	1.524	0.0317
Speed, rpm	1.295	0.0102
g (stager angle, degree)	9,000	30,000
a2 (stator exit angle)	14.7	
b2 (impeller exit angle)	21	
R2 (Impeller exit radius, m)		35
		0.055

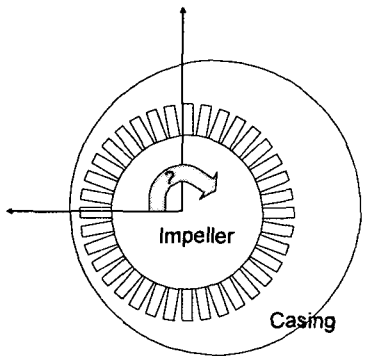

Fig. 1. Asymmetric tip clearance in a circumferential direction.

solution of the flow in a rotating reference frame. Spakovszky [8] renewed axial and radial compressor dynamic system modeling, introducing 'transmission matrix' which can be linked to any other system component to enable efficient and flexible modeling of compression system.

The researches in axial compressors have been conducted much on the field of tip clearance flow, various tip clearance effects on the performance, instability due to tip clearance, and so on. However, the research in centrifugal compressors is very scarce because of the difficulty in an analysis on the radial component, especially, in radial-circumferential plane, even though the tip clearance still plays an important role on the performance and stability. In addition, there is no model which can explain the asymmetric tip clearance effects.

Therefore, the objective of this study is to develop such a model that the tip clearance effects on centrifugal compressor flow can be predict, especially, the nonuniformity by a nonaxisymmetric tip clearance and to understand the effective parameter to affect centrifugal compressor flow.

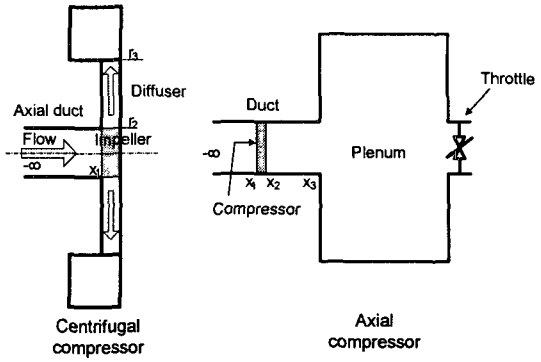

Fig. 2. Schematic view of centrifugal and axial compressors.

2. Model Idescription

This section introduces a newly developed flow model based on "Moore-Greitzer" framework for a centrifugal compressor with radially asymmetric tip clearance as shown in Fig. 1. The model consists of the inlet and exit duct of compressor, combining the flow conditions of two positions with a compressor characteristic curve. For axial compressors, the system consists of the axial duct - compressor - axial duct combination and for centrifugal compressors the axial duct - compressor - radial diffuser. Thus, the flow in this system is assumed 2-dimensional flow, especially, in the axial and circumferential direction for the axial duct and in the radial and circumferential direction for the radial duct. The impeller is modeled as semi-actuator disks to connect the flow in the axial duct and in the radial duct as shown in Fig. 2. The flow in compression system is assumed to be incompressible and inviscid. Test compressors are (1) LSRC at General Electric Aircraft Engines, used by Graf et al. [6] and (2) the SNU centrifugal

compressor with 64 mm inlet diameter and 30,000 rpm, operating in an incompressible region (Ma < 0.3). The details in the facilities are shown in Table. 1. The asymmetry in a tip clearance is modeled as a radial eccentricity without whirling motion.

2.1. Axial duct flow feild

In a centrifugal compressor, the inlet of the impeller can be modeled same as that of an axialcompressor. In that region, the flow is assumed as 2-dimensional flow in axial and circumferential directions. The axial and circumferential velocity perturbations and the pressure perturbation are obtained from the vorticity and the stream function with the vorticity equation and the vorticity definition. In axial duct, the flow is assumed to be 2-dimmensional.

The vorticity equation is shown in Eq. (1)

$$\frac{\partial \omega}{\partial t} + (V \cdot \nabla)\omega = 0 \tag{1}$$

, where ω and V are vorticity and velocity, respectively. This linearized form is the following equation with $\omega = \bar{\varsigma} + \delta\varsigma$ and $\int_0^{2\pi} \delta\varsigma(\theta)d\theta = 0$.

$$\bar{V}_x \frac{\partial \delta\varsigma}{\partial x'} + \bar{V}_\theta \frac{\partial \delta\varsigma}{\partial \theta} = 0 \tag{2}$$

This equation gives a following solution.

$$\delta\varsigma(x,\theta) = \sum_{n=1}^{\infty} \hat{C}_n e^{-jn\frac{\bar{V}_\theta}{\bar{V}_x}x + jn\theta} \tag{3}$$

Introducing a stream function, the vorticity definition gives next relation.

$$\nabla^2\psi = -\omega_z \tag{4}$$

In addition, Eq. (4) is linearized into Eq. (5).

$$\frac{\partial^2 \delta\psi}{\partial x'^2} + \frac{\partial^2 \delta\psi}{\partial \theta^2} = -R^2 \delta\varsigma \tag{5}$$

Substituting the solution of vorticity perturbation into Eq. (5), the solution of stream function perturbation is

$$\delta\psi = \sum_{n=1}^{\infty}\left(\frac{A_n}{jn}e^{nx'} + \frac{B_n}{jn}e^{-nx'} + \frac{C_n}{jn}e^{-jn\frac{\bar{V}_\theta}{\bar{V}_x}x'}\right)\cdot e^{jn\theta} \tag{6}$$

The velocity can be denoted by the stream function, ψ which satisfies the continuity.

$$\delta v_x = \frac{1}{R}\frac{\partial \delta\psi}{\partial \theta} \quad \text{and} \quad \delta v_\theta = -\frac{\partial \delta\psi}{\partial x} \tag{7}$$

The pressure perturbation can be obtained by integrating the axial or circumferential direction momentum equation.

$$\delta P(x,\theta) = \int_{x_0}^{x}\left(-\bar{V}_x \frac{\partial \delta V_x}{\partial x} - \bar{V}_\theta \frac{\partial \delta V_x}{\partial \theta}\right)d\xi \tag{8}$$

Thus, the flow field perturbation solution consists of a sum of harmonic transmission matrices and is written as Eq. (9).

$$\begin{bmatrix} \delta V_x \\ \delta V_\theta \\ \delta P \end{bmatrix} = \sum_{n=1}^{\infty} T_{ax,n} \cdot \begin{bmatrix} A_n \\ B_n \\ C_n \end{bmatrix} \cdot e^{jn\theta} \tag{9}$$

where the n-th harmonic matrices are defined as

$$T_{ax,n} = \begin{bmatrix} e^{nx'} & e^{-nx'} & e^{-jn\frac{\bar{V}_\theta}{\bar{V}_x}x'} \\ je^{nx'} & -je^{-nx'} & \frac{\bar{V}_\theta}{\bar{V}_x}e^{-jn\frac{\bar{V}_\theta}{\bar{V}_x}x'} \\ (-\bar{V}_x - j\bar{V}_\theta)e^{nx'} & (-\bar{V}_x + j\bar{V}_\theta)e^{-nx'} & 0 \end{bmatrix} \tag{10}$$

2.2. Diffuser dynamics

In a centrifugal compressor, the flow enters impeller axially and leaves radially, creating the swirling motion in the diffuser. Because of this reason, the linearized equations should be solved in cylindrical coordinates of radial and circumferential direction. Because of this reason, the flow analysis approach is more complicated than that in the previous section for an axial duct.

The procedure to obtain transmission matrix of the flow in radial duct is similar to that for axial duct dynamics.

From the vorticity equation in cylindrical coordinate, the following Eq. (11) can be obtained.

$$\bar{V}_r \frac{\partial \delta\varsigma}{\partial r} + \frac{\bar{V}_\theta}{r} \frac{\partial \delta\varsigma}{\partial \theta} = 0 \tag{11}$$

The definition of vorticity gives Eq. (12).

$$\frac{\partial^2 \delta\psi}{\partial r^2} + \frac{1}{r} \frac{\partial \delta\psi}{\partial r} + \frac{1}{r^2} \frac{\partial^2 \delta\psi}{\partial \theta^2} = -\delta\varsigma \tag{12}$$

In the radial space of diffuser, the mean velocity can be represented by a free vortex flow as followings.

$$\bar{V}_\theta(r) = \frac{\Gamma}{2\pi r}, \quad \bar{V}_r(r) = \frac{Q}{2\pi r h_2 \rho} \tag{13}$$

,where Γ and Q are the circulation and the flow rate constants, respectively. For the convenience of calculation, $\bar{V}_\theta(r) = \frac{\Gamma}{r}$ and $\bar{V}_r(r) = \frac{Q}{r}$ are denoted.

From Eqs. (11) and (12), the perturbation of stream function can be obtained with a periodic spatial harmonic solution. The radial and circumferential velocity perturbations are from the stream function.

$$\delta v_r = \frac{1}{r} \frac{\partial \delta\psi}{\partial \theta} \quad \text{and} \quad v_\theta = -\frac{\partial \delta\psi}{\partial r} \tag{14}$$

To find the pressure perturbation, the linearized circumferential direction momentum equation is used.

$$-\frac{1}{\rho r} \frac{\partial \delta P}{\partial \theta} = \frac{Q}{r} \frac{\partial \delta v_\theta}{\partial r} + \frac{\Gamma}{r^2} \frac{\partial \delta v_\theta}{\partial \theta} + \frac{Q}{r^2} \delta v_\theta \tag{15}$$

Therefore, the next transmission matrix for swirling flow can be obtained with Eqs. (16).

$$\begin{bmatrix} \delta V_r \\ \delta V_\theta \\ \delta P \end{bmatrix} = \sum_{n=1}^{\infty} T_{rad,n} \cdot \begin{bmatrix} D_n \\ E_n \\ F_n \end{bmatrix} \cdot e^{jn\theta} \tag{16}$$

, where

$$T_{rad,n} = \begin{bmatrix} jnr^{n-1} & jnr^{-n-1} & jn\frac{R_n}{r} \\ -nr^{n-1} & nr^{-n-1} & -\frac{\partial R_n}{\partial r} \\ \left(-\frac{jnQ}{n\Gamma}+\right) r^{n-2} & \left(-\frac{jnQ}{n\Gamma}-\right) r^{-n-2} & \left(\frac{Q}{jn}\frac{\partial^2 R_n}{\partial r^2}+ \frac{1}{jn}\left(\frac{Q}{r}+jn\frac{\Gamma}{r}\right)\frac{\partial R_n}{\partial r}\right) \end{bmatrix} \tag{17}$$

, where

$$R_n = \int_0^{\xi} e^{-jn\frac{\Gamma}{Q}\log\xi} \left(r^n \xi^{-n+1} - r^{-n} \xi^{n+1}\right) d\xi \tag{18}$$

2.3. Impeller actuator dynamics

In this section, the circumferentially nonaxisymmetric tip clearance model is presented. An equation for nonaxisymmetric steady flow through a compressor is as follows.

$$\frac{P_2 - P_{t1}}{\rho U_t^2} = \Psi_{ts} - \lambda_{imp} \frac{d\phi}{d\theta} \tag{19}$$

, where λ_{imp} presents the inertia of the fluid in the impeller passage and is defined:

$$\lambda_{imp} = \frac{AR_{imp} \cdot \log(AR_{imp})}{AR_{imp} - 1} \cdot s_{imp} \tag{20}$$

, where $AR_{imp} = \frac{\rho_2 A_2}{\rho_1 A_1}$ is the impeller area-density ratio and s_{imp} is the mean passage length in the streamwise direction.

The physical content of Eq. (19) is that the local pressure difference across the compressor (exit static minus inlet total) is given by the local uniform flow compressor pumping characteristic plus a correlation to account for the fact that the flow in the impeller, which move through a circumferentially nonuniform flow, has perturbation through a circumferential direction. In Eq. (19), the compressor characteristic utilized is the axisymmetric total-to-static pressure rise coefficient, Ψ_{ts}, as a function of flow coefficient, ϕ. Equation (21) is the

form which Eq. (19) is linearized into.

$$\frac{\delta P_2}{\rho} = U_t^2\left(\frac{\partial \Psi}{\partial \phi}\frac{\delta v_{x1}}{U_t} + \frac{\partial \Psi}{\partial \varepsilon}\delta\varepsilon - \frac{\lambda_{imp}}{U_t}\frac{\partial \delta v_{x1}}{\partial \theta}\right) + \frac{\delta P_1}{\rho} + \overline{V}_{x1}\delta v_{x1} + \overline{V}_{\theta 1}\delta v_{\theta 1} \quad (21)$$

In Eq. (21), the perturbation is presented and $\frac{\partial \Psi}{\partial \phi}$ and $\frac{\partial \Psi}{\partial \varepsilon}$ are the derivatives of the axisymmetric pressure rise characteristics with respect to axial flow coefficient and tip clearance.

By substituting with spatial harmonic solution in Eq. (21), the relation between the perturbationof impeller exit pressure and that of pressure and velocity of impeller inlet is obtained.

The radial velocity at the exit of impeller can be from the continuity.

$$V_{r2} = \frac{1}{AR_{imp}}V_{x1} \quad (22)$$

The circumferential velocity is obtained with the assumption that the flow follows the blades perfectly and blockage and deviation are not accounted for in this model.

$$V_{\theta 2} = U_t - V_{r2}\tan|\beta_2| = V_{r2}\tan\alpha_2 \quad (23)$$

where β_2 and α_2 are a relative exit angle and absolute exit angle, respectively.

The above Eqs. (21), (22) and (23) are linearized and cast into a transmission matrix giving

$$\begin{bmatrix}\delta V_{r2}\\ \delta V_{\theta 2}\\ \delta P_2\end{bmatrix} = \sum_{n=0}^{\infty}\left\{B_{imp,n}\begin{bmatrix}\tilde{v}_{x1,n}\\ \tilde{v}_{\theta 1,n}\\ \tilde{P}_{1,n}\end{bmatrix} + \begin{bmatrix}0\\ 0\\ \frac{\partial \Psi}{\partial \varepsilon}U_t^2\end{bmatrix}\tilde{\varepsilon}_n\right\}e^{jn\theta} \quad (24)$$

The n-th harmonic transmission matrix for a radial impeller is defined as

$$B_{imp,n} = \begin{bmatrix}\frac{1}{AR_{imp}} & 0 & 0\\ \frac{\tan\alpha_2}{AR_{imp}} & 0 & 0\\ \left(U_t\left(\frac{\partial \Psi}{\partial \phi} - jn\lambda_{imp}\right) + \overline{V}_{x1}\right) & \overline{V}_{\theta 1} & 1\end{bmatrix} \quad (25)$$

2.4. Rotor actuator dynamics

The transmission matrix for the rotor actuator dynamics in an axial compressor can be obtained with the same procedure as for the impeller dynamics in a centrifugal compressor.

$$B_{rotor,n} = \begin{bmatrix}1 & 0 & 0\\ \tan\alpha_2 & 0 & 0\\ \left(U_t\left(\frac{\partial \Psi}{\partial \phi} - jn\lambda_{rotor}\right) + \overline{V}_{x1}\right) & \overline{V}_{\theta 1} & 1\end{bmatrix} \quad (26)$$

where α_2 is the stator exit angle.

2.5. Transmission matrix stacking for axial compressors

As shown in Fig. 1, the axial compressor consists of the inlet axial duct, compressor actuator, and the exit axial duct. Therefore, the exit flow parameter can be obtained with the following transmission matrix.

$$\begin{bmatrix}\delta V_{r2}\\ \delta V_{\theta 2}\\ \delta P_2\end{bmatrix} = \sum_{n=0}^{\infty}\left\{B_{rotor,n}\begin{bmatrix}\tilde{v}_{x1,n}\\ \tilde{v}_{\theta 1,n}\\ \tilde{P}_{1,n}\end{bmatrix} + \begin{bmatrix}0\\ 0\\ \frac{\partial \Psi}{\partial \varepsilon}U_t^2\end{bmatrix}\tilde{\varepsilon}_n\right\}e^{jn\theta} \quad (27)$$

The Fourier spatial coefficients for compressor exit velocity and pressure are denoted by the transmission matrix stacking.

$$T_{ax,n}(x_2)\cdot\begin{bmatrix}D_n\\ E_n\\ F_n\end{bmatrix} = B_{imp,n}\cdot T_{ax,n}(x_1)\cdot\begin{bmatrix}A_n\\ B_n\\ C_n\end{bmatrix} + \begin{bmatrix}0\\ 0\\ \frac{\partial \Psi}{\partial \varepsilon}U_t^2\end{bmatrix}\tilde{\varepsilon}_n \quad (28)$$

By taking the inverse of $T_{ax,n}(x_2)$, the Fourier spatial coefficients of exit system can be found.

2.6. Transmission matrix stacking for centrifugal

compressors

As shown in Fig. 1, the flow passes through an axial duct, impeller, and aradial diffuser. Thus, the perturbation relationship between the inlet flow and exit flow can be obtained with Eqs. (9), (16), and (24).

$$\begin{bmatrix} \delta V_{r2} \\ \delta V_{\theta 2} \\ \delta P_2 \end{bmatrix} = \sum_{n=0}^{\infty} \left\{ B_{imp,n} \begin{bmatrix} \tilde{v}_{x1,n} \\ \tilde{v}_{\theta 1,n} \\ \tilde{P}_{1,n} \end{bmatrix} + \begin{bmatrix} 0 \\ 0 \\ \frac{\partial \Psi}{\partial \varepsilon} U_t^2 \end{bmatrix} \tilde{\varepsilon}_n \right\} e^{jn\theta} \quad (29)$$

Focusing on only n-th harmonic spatial Fourier coefficients,

$$T_{rad,n}(r_2) \cdot \begin{bmatrix} D_n \\ E_n \\ F_n \end{bmatrix} = B_{imp,n} \cdot T_{ax,n}(x_1) \cdot \begin{bmatrix} A_n \\ B_n \\ C_n \end{bmatrix} + \begin{bmatrix} 0 \\ 0 \\ \frac{\partial \Psi}{\partial \varepsilon} U_t^2 \end{bmatrix} \tilde{\varepsilon}_n \quad (30)$$

2.7. Boundary conditions

In the axial duct, no vorticiy will be present in the entire upstream region since vortical motion can only be propagated in the flow direction and no vorticity is created upstream of the compressor. Therefore it is appropriate to set $C_n = 0$ in the upstream region. At far upstream of compressor, the potential perturbation should be zero since the compressor is only energy source. Thus, B_n should be zero. At the downstream of compressor, the volute dimensions are much larger than compressor diffuser. This reason enables to assume the flow at the diffuser exit is approximately spatially uniform.

$$\tilde{P}_3 = \left[T_{rad,n}(3,1) \;\; T_{rad,n}(3,2) \;\; T_{rad,n}(3,2) \right] \cdot \begin{bmatrix} D_n \\ E_n \\ F_n \end{bmatrix} = 0 \quad (31)$$

Therefore, the 4 unknown spatial coefficients (A_n, D_n, E_n, and F_n) exist and 3 equations from the 3 components of the transmission matrix from Eq. (30) and 1 equation from Eq. (31) exist.

3. Discussion

To validate this model, theresults by Graf et al. [6] are used in this axial compressor model. Figure 3. shows the characteristics of the test compressor for 3 different axisymmetric tip clearances. Graf et al. [6] tested with the one-lobed and the two-lobed tip clearance geometries of ±1.4% of a chord length. Figures 5 and 6 show the flow coefficient nonuniformity along circumferential direction for the one-lobed tip clearance and the two-lobed tip clearance, respectively. The exact tip clearance geometry is shown on the bottom in each figure. As the flow coefficient decreases, the magnitude of flow coefficient by both the experiment and this modeling results are increased for both the one-lobed and the two-lobed tip clearances. In addition, the flow coefficient is the highest where the tip clearance is

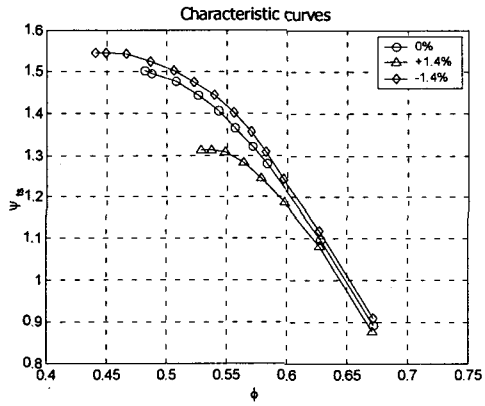

Fig. 3. Characteristics for the axial compressor (Graf et al. [6]).

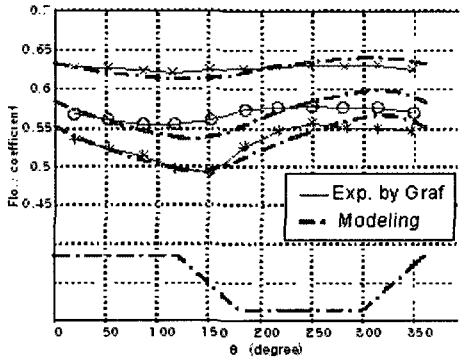

Fig. 4. Flow coefficient variation for the one lobe asymmetry, compared with Graf el al. [6].

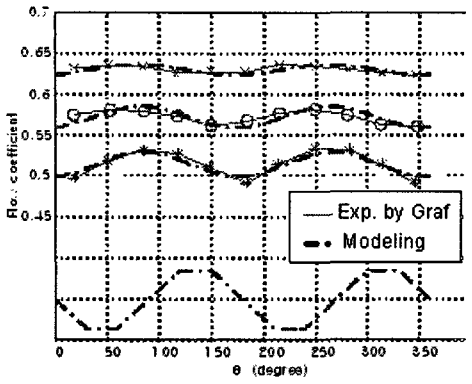

Fig. 5. Flow coefficient variation for the two lobe asymmetry, compared with Graf el al. [6].

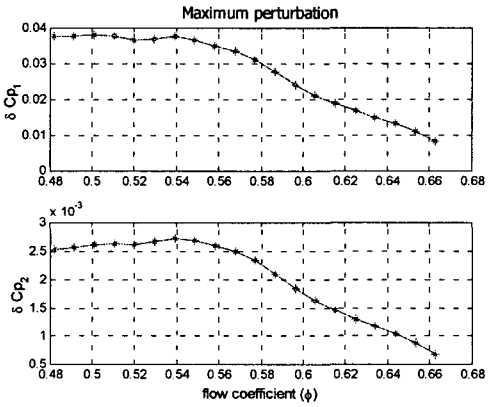

Fig. 6. Pressure perturbations at the inlet and the exit of the axial compressor.eccentricity for the centrifugal compressor used in this model.

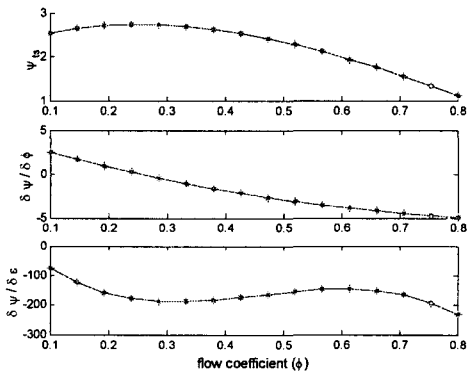

Fig. 7. Compressor characteristic and the slopes with respect to flow coefficient and eccentricity for centrifugal compressor.

getting larger. These two figures show the good match in the magnitude and phase with these modeling results. Figure 6. shows the pressure perturbation vs. flow coefficient at the inlet and the exit of the axial compressor. As flow coefficient decreases, the magnitude of perturbation is also increased. In addition, the pressure nonuniformity is decreased from compressor inlet to exit.

Figure 7. shows the total-to-static compressor characteristic and the slopes by flow coefficient and Figure 8. shows the inlet and exit velocity nonuniformities in the centrifugal compressor. In the centrifugal compressor, the velocity nonuniformity shows a same trend with that of the axial compressor. The maximum value of inlet velocity exits right before the maximum tip clearance.

Figure 9. shows the pressure nonuniformities at the inlet and exit of the impeller in the centrifugal compressor. In the inlet, the total pressure uniforms

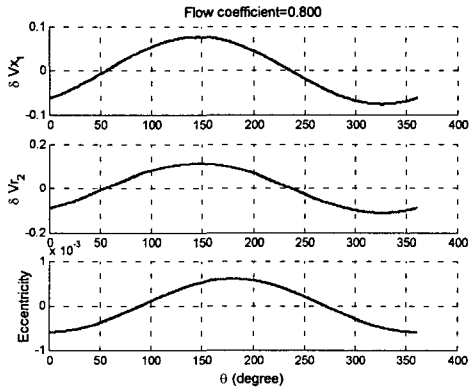

Fig. 8. The nonuniformity of the inlet and exit velocity in centrifugal compressor.

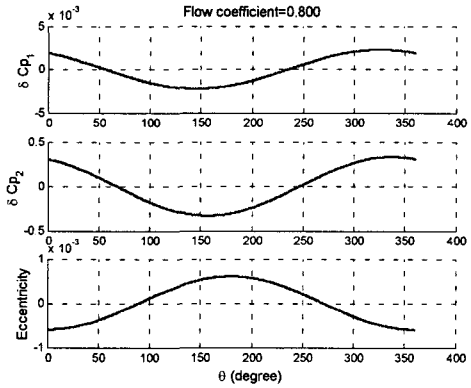

Fig. 9. pressure nonuniformities at the inlet and exit of the impeller in the centrifugal compressor.

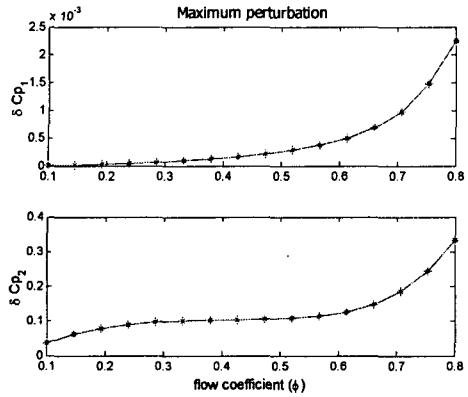

Fig. 10. Magnitude of pressure nonuniformity vs. flow coefficient for centrifugal compressor.

along circumferential direction becauseno work at the upstream of the impeller. Thus, the phase of the pressure nonuniformity shows 180 degree difference with that of the velocity nonuniformity as presented in Fig. 8.

Shown in Fig. 10, the nonuniformity of impeller inlet and exit pressure is decreased as the flow coefficient decreases, contrary to that of axial compressor. In addition, the only exit pressure shows the opposite trend to the slope of pressure coefficient by eccentricity. Also, contrary to the axial compressor shown in Fig. 6, the magnitude of the impeller exit pressure nonuniformity for centrifugal compressor is biggerthan that of the inlet pressure nonuniformity. This shows the possibility to explain why the axial compressor stalls usually at the inlet of rotor and the centrifugal compressor stalls at the diffuser inlet. creases, the magnitude of pertubation comrpessor

4. Conclusions

The following conclusions are reduced by this research.

1. The new model for asymmetric tip clearance for both axial and centrifugal compressor has been developed.

2. The nonuniformity of rotor exit pressure is increased as flow coefficient decreases.

3. Contrary to axialcompressors, the nonuniformity of impeller exit in centrifugal compressordecreases as flow coefficient decreases.

4. The maximum velocity of the inlet of rotor/impeller exists right before the maximum tip clearance.

5. The only exit pressure is sensitive to the slope of pressure rise by the eccentricity.ip clearance for both axial and centrifugal compressor has been developed.ifugal compressor.

6. The magnitude of the impeller exit pressure nonuniformity for centrifugal compressor is bigger than that of the inlet pressure nonuniformity.

5. References

[1] Thomas, H. J., 1958, "Unstable Natural Vibration of Turbine Rotors Induced by the Clearance Flow in Glands and Blading," Bull. De I'A.I.M., Vol. 71, 11/12, pp. 1039-1063.

[2] Alford, J., 1965, "Protecting Turbomachinery from Self-Excited Rotor Whirl," ASME Journal of Engineering for Power, Vol. 87, pp. 333-334.

[3] Greitzer, E. M., 1976, "Surge and Rotating Stall in Axial Compressors; Part I: Theoretical Compression System Model," ASME Journal of Engineering for Power, Vol. 98, pp. 190-198.

[4] Moore, F. K. and Greitzer, E. M., 1986, "A Theory of Post-Stall Transients in Axial Compressors: Part I Development of the Equations,"ASME Journal of Engineering for Gas Turbines and Power, Vol. 108, pp. 68-76.

[5] Hynes, T. P. and Greitzer, E. M., 1987, "A Method for Assessing Effects of Circumferential Flow Distortion on Compressor Stability," ASME Journal of Turbomachinery, Vol. 109, pp. 371-379.

[6] Graf, M. B., Wong, T. S., Greitzer, E. M., Tan, C. S., Shin. H.-W., and Wisler, D. C., 1998, "Effects of Nonaxisymmetric Tip Clearance on Axial Compressor Performance and Stability," ASME Journal of Turbomachinery, Vol. 120, pp. 648-661.

[7] Gordon, K., 1999, "Three-Dimensional Rotating Stall Inception and Effects of Rotating Tip Clearance Asymmetry in Axial Compressors," PhD thesis, Department of Aeronautics and Astronautics, MIT.

[8] Spakovszky. Z. S., 2001, "Applications of Axial and Radial Compressor Dynamic System Modeling," PhD thesis, Department of Aeronautics and Astronautics, MIT.